

# Graphene-Coated Fractal Wideband 5G Microstrip Patch Antenna: Design, Fabrication, and Experimental Validation

Beyza Nur Demirkoparan<sup>1</sup> , Ali Altuntepe<sup>2</sup> , Emre Biçer<sup>3</sup> , Husnu Deniz Basdemir<sup>4</sup> 

<sup>1</sup>Department of Electrical-Electronic Engineering, Sivas University of Science and Technology Faculty of Engineering and Natural Sciences, Sivas, Türkiye

<sup>2</sup>Optical Excellence Application and Research Center, Sivas University of Science and Technology, Sivas, Türkiye

<sup>3</sup>Department of Fundamental Engineering Sciences, Sivas University of Science and Technology Faculty of Engineering and Natural Sciences, Sivas, Türkiye

<sup>4</sup>Department of Electrical and Electronics Engineering, Gazi University Faculty of Engineering, Ankara, Türkiye

**Cite this article as:** B. N. Demirkoparan, A. Altuntepe, E. Biçer and H. D. Basdemir, "Graphene-coated fractal wideband 5G microstrip patch antenna: design, fabrication, and experimental validation," *Electrica*, 2026, 26, 0228, doi:10.5152/electrica.2026.25228.

## WHAT IS ALREADY KNOWN ON THIS TOPIC?

- *Wideband microstrip patch antennas (MPAs) with fractal geometries have been extensively investigated for modern wireless communication systems, particularly 5G, due to their compact size, multiband operation, and good radiation efficiency. Fractal designs, such as those incorporating deterministic geometric scaling and slotting, are known to enhance miniaturization and bandwidth without significantly degrading performance. In parallel, graphene-based conductive coatings, including reduced graphene oxide (rGO), have gained attention for their exceptional electrical conductivity, flexibility, and potential to improve antenna impedance matching*

## Corresponding author:

Husnu Deniz Basdemir

## E-mail:

denizbasdemir@gmail.com

**Received:** August 12, 2025

**Revision Requested:** September 25, 2025

**Last Revision Received:** October 28, 2025

**Accepted:** November 4, 2025

**Publication Date:** February 23, 2026

**DOI:** 10.5152/electrica.2026.25228



Content of this journal is licensed under a Creative Commons Attribution-NonCommercial 4.0 International License.

## ABSTRACT

This paper presents the design, simulation, fabrication, and experimental characterization of a graphene-coated fractal microstrip patch antenna intended for 5G wideband (3–12 GHz) applications. The antenna employs fractal geometries inspired by graphene's hexagonal lattice to achieve compactness and multiband behavior. Two substrate types, FR (flame retardant)-4 and Rogers RT (Rogers series high frequency laminates)-5880, were used to assess performance variations. Reduced graphene oxide (rGO) was synthesized via a modified Hummers method and deposited onto the antenna surfaces using electrophoretic deposition. Simulation results demonstrated excellent impedance matching  $S_{11}$  values of  $-24$  dB (FR-4) and  $-27.9$  dB (Rogers RT-5880), with a peak simulated gain of 4.1 dBi. Experimental measurements confirmed improved performance with rGO coating, achieving  $-27.63$  dB at 9.15 GHz for FR-4 and  $-27.1$  dB at 11.1 GHz for Rogers RT-5880. These findings demonstrate that this integration, novel in its experimental approach, successfully mitigates surface wave losses at higher frequencies and significantly enhances antenna performance for next-generation wireless communication systems.

**Index Terms**—5G communication, electrophoretic deposition (EPD), fractal antenna, graphene, microstrip patch antenna, reduced graphene oxide (rGO), wideband antenna

## I. INTRODUCTION

Fifth-generation (5G) wireless communication systems demand compact, low-profile, wideband, and high-efficiency antennas capable of supporting high data rates and low latency over diverse frequency bands [1]. Among various antenna technologies, microstrip patch antennas (MPAs) are widely preferred due to their planar form factor, ease of integration with monolithic microwave integrated circuits, low fabrication cost, and suitability for mass production [2]. However, traditional MPAs often suffer from limited bandwidth, significant surface wave losses at higher frequencies, and challenges in achieving multiband operation without increasing size or complexity [3-9].

In microstrip antenna design, techniques to improve efficiency and bandwidth have been developed. Increasing substrate thickness is a common method to achieve high efficiency (90%) and a wider bandwidth (around 35%). However, this can lead to surface waves, which reduce radiation efficiency and degrade radiation patterns and polarization. To address this, resonant cavity structures and stacking microstrip elements are used. Despite these advancements, challenges such as large size at lower frequencies, high electromagnetic signatures at off-resonant frequencies, and trade-offs between bandwidth and scanning capability remain, especially for critical 5G applications [10-15]. Fractal geometries have emerged as an effective solution for antenna miniaturization and multiband performance. Their self-similar, space-filling properties enable the design of compact antennas with extended bandwidth and multi-resonance characteristics while maintaining desirable radiation patterns [16].

and bandwidth. Previous studies have demonstrated that combining advanced substrate materials with optimized antenna geometries can further enhance high-frequency performance.

## WHAT THIS STUDY ADDS TO THIS TOPIC?

- *Theoretical justification:* Detailed justification of the hexagonal fractal structure's impedance matching and multi-resonance effects. This is the first reported experimental study to successfully integrate a rGO conductive layer onto a fractal MPA using electrophoretic deposition for enhanced wideband 5G performance.
- *Comparative analysis:* A rigorous comparison of rGO-coated fractal antennas on two distinct substrates (FR-4 and Rogers RT-5880) to evaluate material-dependent performance.
- *High-frequency enhancement:* Demonstration and analysis of rGO's unique ability to significantly improve return loss  $S_{11}$  at high 5G frequency bands (up to 12 GHz), offering a clear advantage over conventional copper conductors in reducing surface wave losses.

Additionally, advanced materials such as graphene have attracted significant attention for antenna applications due to their exceptional electrical conductivity, mechanical strength, and tunable electromagnetic properties [17-20]. In particular, reduced graphene oxide (rGO) coatings can enhance surface conductivity and reduce resistive losses at high frequencies [21]. Despite substantial theoretical and simulation-based research on graphene-based antennas, experimental demonstrations at GHz frequencies remain relatively limited. Furthermore, few studies have explored the integration of graphene coatings with fractal microstrip geometries for wideband 5G applications [22-27]. This work addresses this gap by presenting the design, simulation, fabrication, and experimental characterization of a graphene-coated fractal MPA covering the 3–12 GHz band.

The proposed antenna employs fractal patterns inspired by the atomic-scale hexagonal structure of graphene, enabling broadband operation while maintaining compact dimensions. Two substrate materials, FR-4 and Rogers RT-5880, were used to investigate the impact of dielectric properties on antenna performance. Reduced graphene oxide was synthesized via a modified Hummers method and deposited onto the antenna surfaces using electrophoretic deposition (EPD). Simulation and real-time measurement results demonstrate that the integration of fractal structures and rGO coatings significantly improves impedance matching and return loss at higher frequencies, making the design a promising candidate for next-generation 5G communication systems.

## II. ANTENNA DESIGN AND FABRICATION

### A. Antenna Geometry and Design

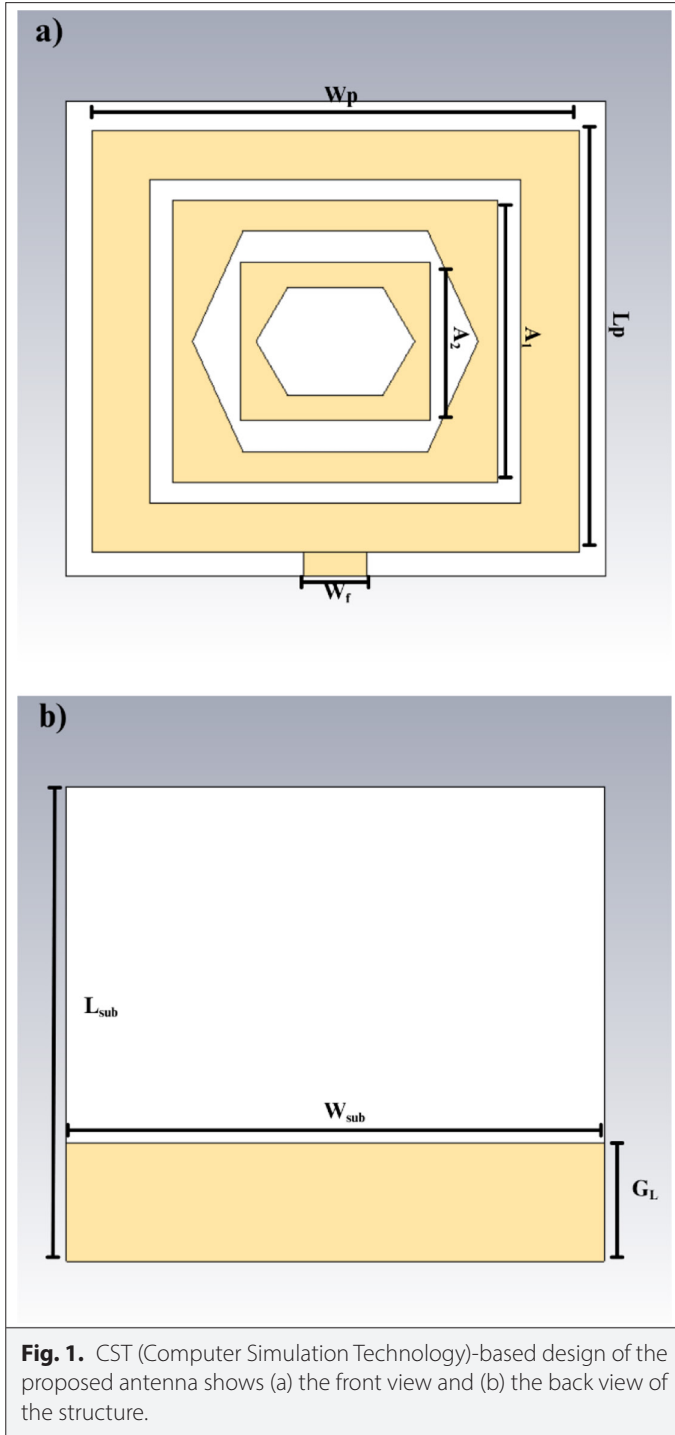
The proposed antenna utilizes a fractal geometry inspired by the self-similarity principle to maximize the electrical length within a constrained physical area. Specifically, the hexagonal notch geometry was chosen (Fig. 1). This structure is theoretically advantageous over conventional square or rectangular fractals because the hexagonal iteration efficiently increases the path of the surface current, thereby lowering the resonant frequency and facilitating multiple resonance bands necessary for wideband operation. Furthermore, the hexagonal notches introduce inductive and capacitive loadings that help maintain optimal impedance matching  $Z_{in} \approx 50 \Omega$  across a wider frequency range. The final optimized dimensions for the antenna are presented in Table I.

The antenna geometry was modeled using CST Microwave Studio, allowing full-wave simulation of the electromagnetic fields and optimization of key parameters. Design refinements included adjusting the slot dimensions and feed location to enhance impedance matching and minimize reflection loss ( $S_{11}$ ) across the targeted frequency range. A partial ground plane was employed to further broaden the bandwidth and improve the radiation efficiency. The proposed antenna was designed as a microstrip patch structure incorporating fractal geometries to achieve wideband performance in the 3–12 GHz range. The design process was carried out using CST Microwave Studio software, which enabled precise modeling of the antenna geometry and electromagnetic properties. The antenna features a square patch with fractal slots inspired by the hexagonal lattice structure of graphene, facilitating multiband operation while maintaining compact dimensions. Under a semi-classical, local model and in the absence of an external magnetic field, graphene's conductivity can be modeled using the intraband contribution of the Kubo formula given in (1) [28]:

$$\sigma = -j \frac{e^2 k_B T}{\pi \hbar^2 (\omega - j\tau^{-1})} \ln \left\{ 2 \left[ 1 + \cosh \left( \frac{\mu_c}{k_B T} \right) \right] \right\} \quad (1)$$

where:

- $e$  is elementary charge,
- $k_B$  is the Boltzmann constant,
- $T$  is the absolute temperature,
- $\hbar$  is reduced Planck constant,
- $\omega$  is angular frequency,
- $\tau$  is relaxation time,
- $\mu_c$  is chemical potential (Fermi energy) [29].



To ensure accurate modeling of the antenna, the dimensions of the microstrip patch must be calculated precisely. The design consists of a square patch positioned on a dielectric substrate with a relative permittivity ( $\epsilon_r$ ) placed above a perfect electric conductor ground plane. The patch, assumed to be made of copper, is excited via a copper microstrip feed line. For microstrip antennas, the width-to-height ratio should satisfy  $W/h > 1$ . When  $W/h > 1$ , surface wave excitation is reduced, and radiation efficiency increases [30]. The effective dielectric constant is given in (2) [28]. The effective dielectric constant is nearly constant at low frequencies. Its values start

**TABLE I.** OPTIMIZED ANTENNA DIMENSIONS

Parameter	Value (mm)	Description
$W_p$	15.36	Patch width
$L_p$	13.3	Patch length
$L_{sub}$	15	Substrate length
$W_{sub}$	17	Substrate width
$h$	1.6	Substrate thickness (FR-4)
$W_f$	2	Feed line width (50 $\Omega$ )
$G_L$	3.75	Partial ground plane length
$A_1$	11.82	Side length of the first hexagonal notch
$A_2$	8,87	Side length of the second hexagonal notch

to rise monotonically at intermediate frequencies and finally get close to the substrate's dielectric constant values. The static values are the initial values of the effective dielectric constant (at low frequencies).

$$\epsilon_{reff} = \frac{\epsilon_r + 1}{2} + \frac{\epsilon_r - 1}{2} \left[ 1 + 12 \frac{h}{w} \right]^{-1/2} \quad (2)$$

The calculation of width ( $W$ ) of the patch is given in (3) is then determined using [28]:

$$W = \frac{1}{2f_r \sqrt{\mu_0 \epsilon_0}} \sqrt{\frac{2}{\epsilon_r + 1}} = \frac{v_0}{2fr} \sqrt{\frac{2}{\epsilon_r + 1}} \quad (3)$$

Once  $W$  is calculated, the length extension  $\Delta L$ , caused by fringing effects, is computed as in (4) [28].

$$\frac{\Delta L}{h} = 0.412 \frac{(\epsilon_{reff} + 0.3) \left( \frac{w}{h} + 0.264 \right)}{(\epsilon_{reff} - 0.258) \left( \frac{w}{h} + 0.8 \right)} \quad (4)$$

Finally, the effective length of the  $L$  of the patch is calculated using in (5) [28].

$$L = \frac{1}{2f_r \sqrt{\epsilon_{reff}} \sqrt{\mu_0 \epsilon_0}} - (2\Delta L) \quad (5)$$

## B. Substrate Materials

Two different substrate materials were selected to investigate the impact of dielectric properties on antenna performance. FR-4, with a relative permittivity ( $\epsilon_r$ ) of 4.3 and a thickness of 1.6 mm, offers low cost and widespread availability but exhibits higher dielectric losses at microwave frequencies. In contrast, Rogers RT-5880 features a lower  $\epsilon_r$  of 2.2 and a low-loss tangent, making it more suitable for high-frequency applications. For each substrate, the patch dimensions were analytically calculated using microstrip antenna design equations, accounting for the effective dielectric constant and fringing fields to ensure proper resonance behavior within the 5G band.

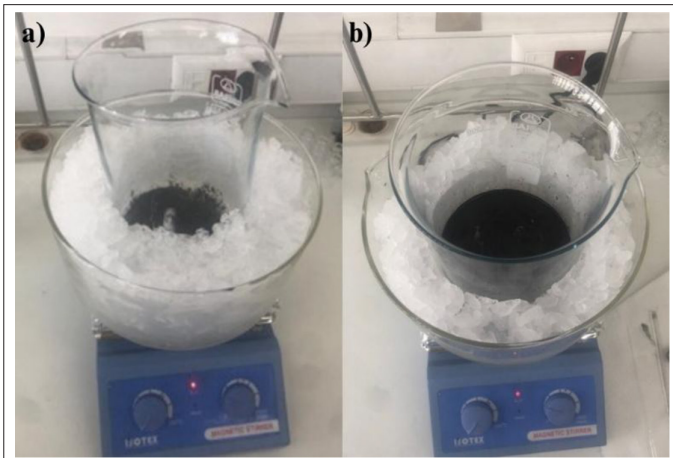


**Fig. 2.** Mixing phase of graphite powder and sulfuric acid in the ice bath (a), the formation phase of graphite oxide left to stir in an ice bath (b) [32].

### C. Reduced Graphene Oxide Synthesis

Graphene oxide (GO) was synthesized from graphite powder using a modified Hummers method to enable its subsequent reduction to rGO for antenna coating. The process involved mixing graphite with sodium nitrate and slowly adding concentrated sulfuric acid under continuous stirring to initiate oxidation. Potassium permanganate was then gradually introduced while maintaining the temperature below 20°C to control exothermic reactions. After further stirring at 35°C for 12 hours, the reaction mixture was diluted with deionized water and treated with hydrogen peroxide to complete oxidation and exfoliation, producing a characteristic color change indicating GO formation [31]. Figs. 2 and 3 capture the key stages of the reaction and separation process. The resulting solution was washed with hydrochloric acid and deionized water to remove impurities, then filtered and dried to yield fine GO powder. Finally, the GO was chemically reduced using hydrazine hydrate to obtain rGO with improved electrical conductivity. This rGO was subsequently dispersed in a suitable solvent for EPD onto the antenna surfaces, enabling uniform, conductive coatings that enhance high-frequency antenna performance.



**Fig. 3.** Graphite oxide that settles to the bottom because of resting (a), the ultrasonic bathing phase of graphite oxide (b) [32].

Graphene was dispersed in various polar and non-polar solvents, including water, chloroform, carbon tetrachloride, and hexane, to evaluate dispersion behavior and achieve stable suspensions for coating applications. Ultrasonic treatment was used to overcome Van der Waals forces between sheets, improving exfoliation and dispersion uniformity [33]. To further enhance colloidal stability and prevent agglomeration, different dispersing agents such as anionic surfactants (e.g., sodium dodecylbenzenesulfonate), polyelectrolytes (e.g., sodium lignosulfonate), classical surfactants (e.g., cetyltrimethylammonium bromide), and water-soluble polymers (e.g., Polyvinylpyrrolidone (PVP) and Polyvinyl Alcohol (PVA)) were employed based on their interaction potential with graphene surfaces. Dispersions were visually inspected for homogeneity before use in EPD processes.

Reduced graphene oxide (rGO) was obtained by chemically reducing GO synthesized via the modified Hummers method. Dry GO powder was dispersed in distilled water with magnetic stirring and ultrasonication to ensure homogeneity. Hydrazine hydrate was added as the reducing agent at a 1:1 weight ratio relative to GO, with reactions conducted at temperatures ranging from 15°C to 95°C to study temperature effects on reduction efficiency. Continuous stirring and sonication helped maintain dispersion and prevent aggregation. After reduction, the rGO was collected by vacuum filtration, washed thoroughly with distilled water to remove residual reagents, and dried at 60°C to yield fine black powder suitable for subsequent coating applications (Fig. 4) [34].



**Fig. 4.** Reduced graphene oxide formed from drying in the oven [32].

To evaluate reproducibility, three identical EPD experiments were conducted. The coating thickness and conductivity varied by less than 5%, confirming repeatability. Industrial scalability has been discussed referencing recent EPD literature [34, 35].

#### D. Electrophoretic Deposition of Reduced Graphene Oxide

Electrophoretic deposition was performed at room temperature using a custom-built electrochemical cell designed for planar substrates such as MPAs. The system employed a two-electrode configuration with the antenna serving as the working electrode (anode) and an iron wire as the counter electrode (cathode), spaced 10 cm apart to ensure uniform electric field distribution. A homogeneous suspension of rGO and copper particles in a suitable solvent served as the electrolyte, maintained under continuous magnetic stirring to prevent sedimentation. Deposition was carried out by applying a controlled DC voltage for optimized durations, enabling negatively charged rGO and copper particles to migrate and uniformly deposit onto the FR-4 substrate surface. Varying voltage and time settings were systematically explored to study their effects on coating uniformity and thickness [35].

To optimize the EPD parameters, a systematic series of experiments was performed in which rGO was deposited onto the antenna surface under varying voltages and durations. This process is shown in Fig. 5. The applied voltage was adjusted across six levels (10 V, 15 V, 20 V, 30 V, 40 V, and 50 V), while deposition times were varied at 80, 120, 240, and 300 minutes. This experimental matrix enabled the evaluation of electric field strength and deposition time effects on film adhesion, uniformity, and thickness. All trials were conducted under consistent environmental conditions with continuous magnetic stirring to maintain colloidal stability and ensure reproducible, high-quality rGO coatings.

After completing the EPD process, the coated antenna samples were removed from the deposition cell and thoroughly rinsed with deionized water to remove residual electrolytes or loosely bound particles. The samples were air-dried at room temperature to eliminate surface moisture before undergoing thermal treatment. Subsequently, they were placed in a convection oven at 70°C for 30 minutes to ensure uniform solvent evaporation and improve rGO layer adhesion and structural stability. This controlled drying step helped prevent thermal degradation or delamination of the rGO coating on both FR-4 and Rogers RT-5880 substrates, preparing the samples for further characterization.

The reproducibility and scalability of the rGO coating via EPD were carefully considered during the experimental design. The EPD

process parameters—such as rGO concentration, applied voltage (10–50 V), deposition time (80–300 minutes), and electrode spacing (10 cm)—were systematically optimized and repeated under identical environmental conditions. Repeated depositions under the same conditions yielded coating thickness variations within  $\pm 5\%$ , confirming good reproducibility across multiple samples. Regarding scalability, EPD is inherently adaptable to large-area and batch manufacturing due to its low-temperature, solution-based nature and compatibility with planar substrates such as FR-4 and Rogers RT-5880.

After EPD, the coated samples were characterized using Raman spectroscopy and scanning electron microscopy (SEM). Film thickness on FR-4 substrates was measured via optical interferometry and SEM imaging (Fig. 6). Raman spectra confirmed successful rGO deposition, with clear D and G peaks observed at  $\sim 1330\text{ cm}^{-1}$  and  $\sim 1590\text{ cm}^{-1}$ , respectively, in samples 1 and 2. The increased D-peak intensity and calculated ID/IG ratios of 1.13 and 1.18 indicated defect introduction consistent with the GO reduction process. Scanning electron microscopy analysis further revealed uniform rGO coverage between copper crystals in samples 1 and 3, confirming good adhesion and film continuity. These results collectively verify the formation of conductive rGO coatings suitable for enhancing antenna performance.

The thickness of the coatings obtained through EPD was quantitatively evaluated using two distinct characterization techniques: optical interferometry and SEM cross-sectional analysis. These complementary methods assessed the surface profile and the internal structural integrity of the deposited rGO layers. Based on optical interferometry measurements, Sample 1 exhibited a coating thickness of 1.5–2.0  $\mu\text{m}$ , whereas Sample 3 demonstrated a relatively thicker layer, ranging from 3.0 to 4.0  $\mu\text{m}$ . These measurements reflect the average vertical displacement across the coated surface under white-light interference conditions.

In contrast, the SEM cross-sectional imaging yielded differing results. For Sample 1, the measured coating thickness varied between 3.74 and 4.88  $\mu\text{m}$ , while Sample 3 exhibited a thinner deposition, with

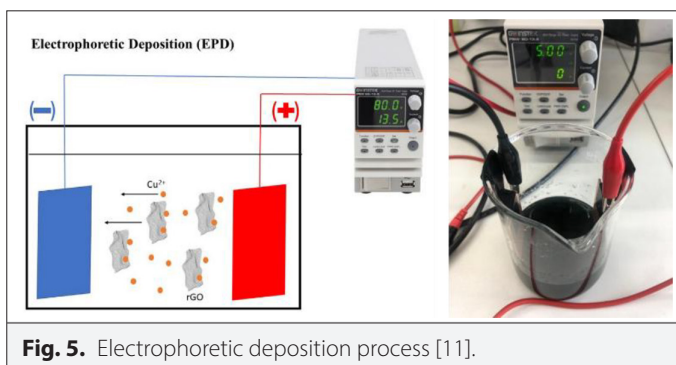


Fig. 5. Electrophoretic deposition process [11].

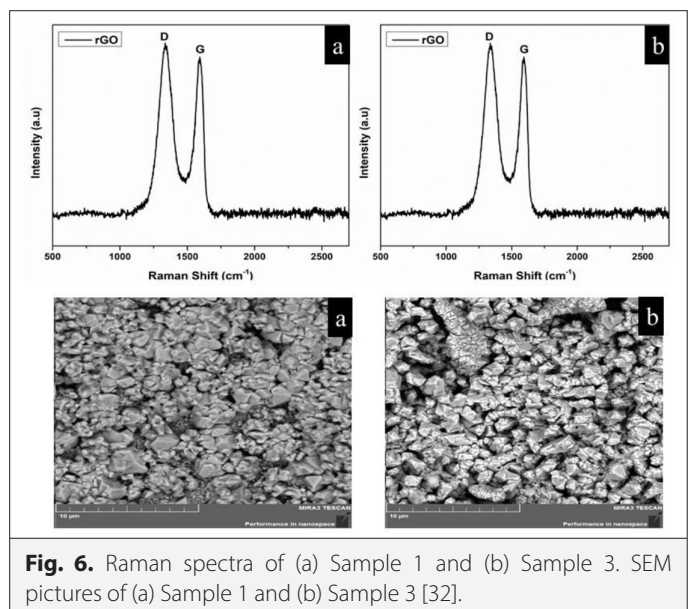
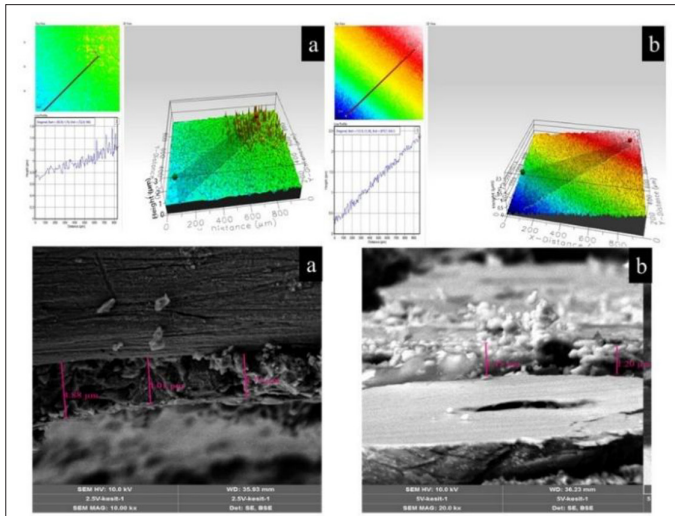


Fig. 6. Raman spectra of (a) Sample 1 and (b) Sample 3. SEM pictures of (a) Sample 1 and (b) Sample 3 [32].



**Fig. 7.** Optical interferometer analysis of (a) Sample 1 and (b) Sample 3. Scanning electron microscopy cross-sectional thickness measurement results: (a) Sample 1 and (b) Sample 3 [32].

values ranging from 1.20 to 1.45  $\mu\text{m}$  (as illustrated in Fig. 7). The discrepancy between the results obtained via the two methods can be primarily attributed to surface roughness and non-uniformity at different regions of the samples. While optical interferometry provides a broader surface average, SEM offers highly localized, high-resolution sectional data, which may capture thinner or thicker areas depending on the selected cross-sectional plane.

These differences highlight the importance of employing multiple complementary techniques for accurately characterizing nanostructured films deposited on non-ideal or heterogeneous surfaces.

Reduced graphene oxide used in the experiments was synthesized by the research group. So, all the electrical properties cannot be measured. Only the SEM pictures and explanations, Raman spectra about the synthesized rGO values, and thickness measurement were carried out.

### E. Fabrication of Antenna

Fig. 8 shows the step-by-step fabrication of the antenna prototypes using the etching process and graphene coating. In Fig. 8a, the raw, unprocessed copper plate is displayed as the starting material before any patterning. Fig. 8b depicts the etched copper pattern created by removing unwanted copper after transferring the antenna design. This etched surface was then coated with rGO via EPD to improve conductivity and reduce resistive losses. Fig. 8c presents the shaping process for the Rogers RT-5880 substrate, highlighting its preparation through precise mechanical or laser machining to match the design specifications. Finally, Fig. 8d shows the fully fabricated graphene-coated RT-5880 antenna, combining advanced low-loss substrate properties with the conductive rGO layer to enhance bandwidth and performance for wideband and 5G mid-band applications.

The preliminary stages of this study were presented in a paper at ELECO 2024. In the following stages, additional data were incorporated, which will be described in this section. Subsequently, a further paper expanding on this work was presented at ICADA 2025. By the final stage of the study, all simulations and real-time measurements had been completed and compared. Measurements and simulation

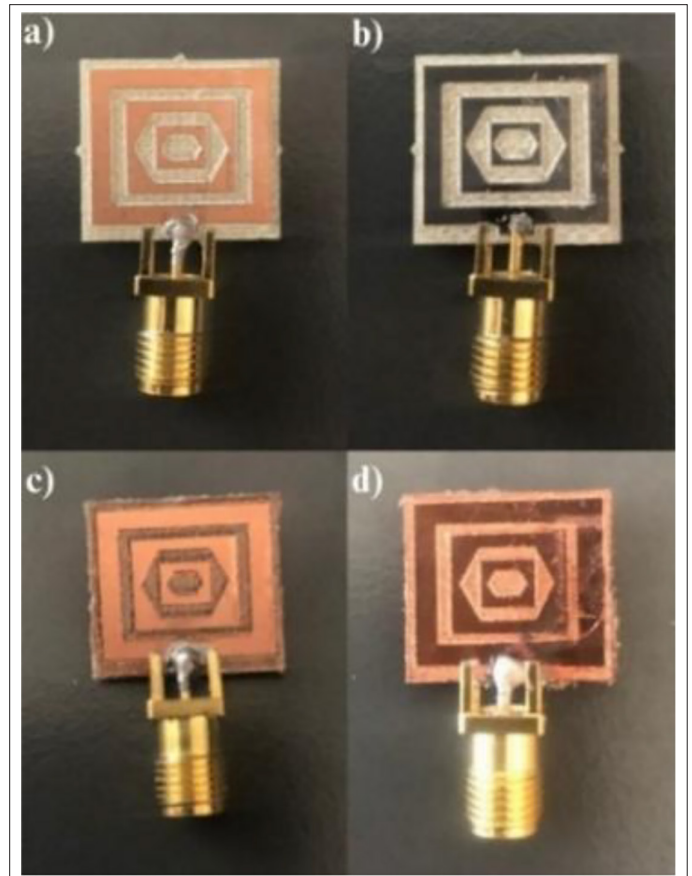


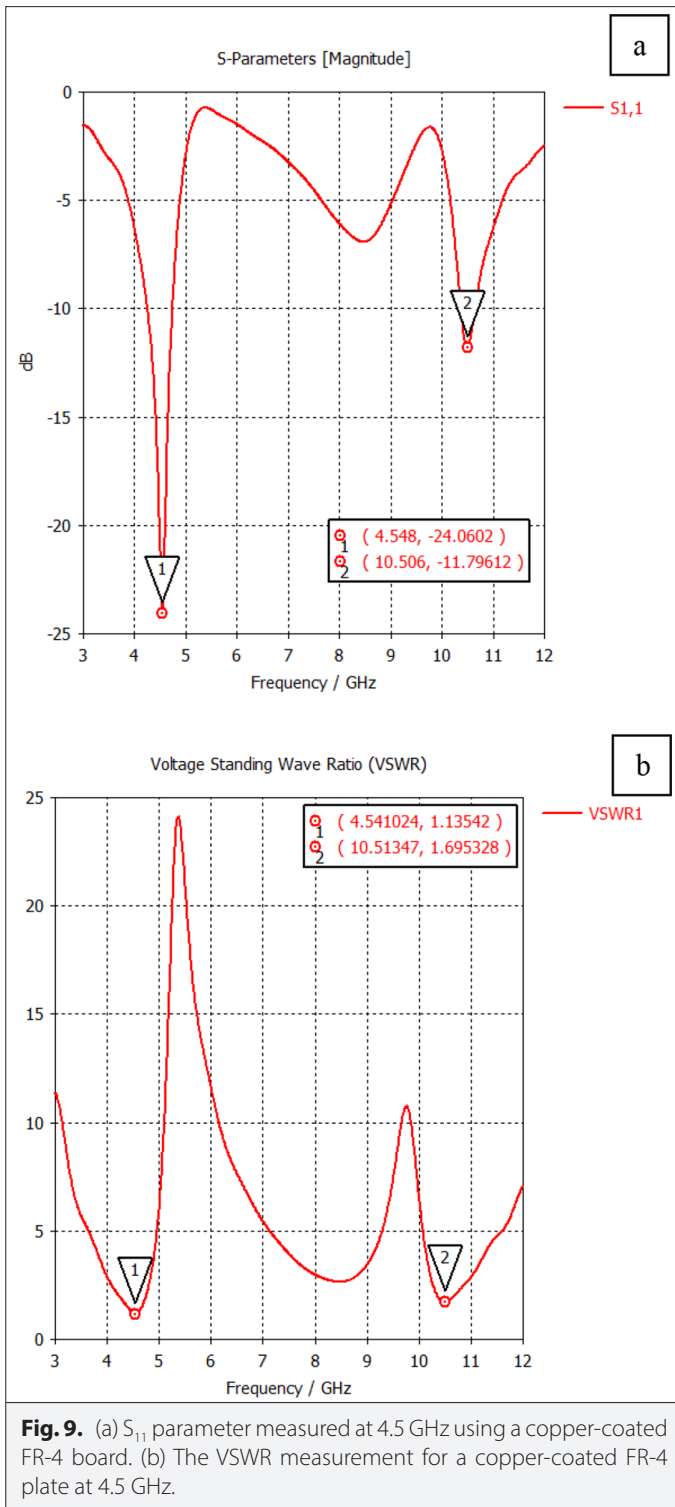
**Fig. 8.** Fabricated prototype of the designed antenna. (a) Only a copper-coated FR-4 plate. (b) Graphene-coated FR-4 plate. (c) Only a copper-coated Rogers RT-5880. (d) Graphene-coated Rogers RT-5880.

results obtained using two different substrates are explained in detail.

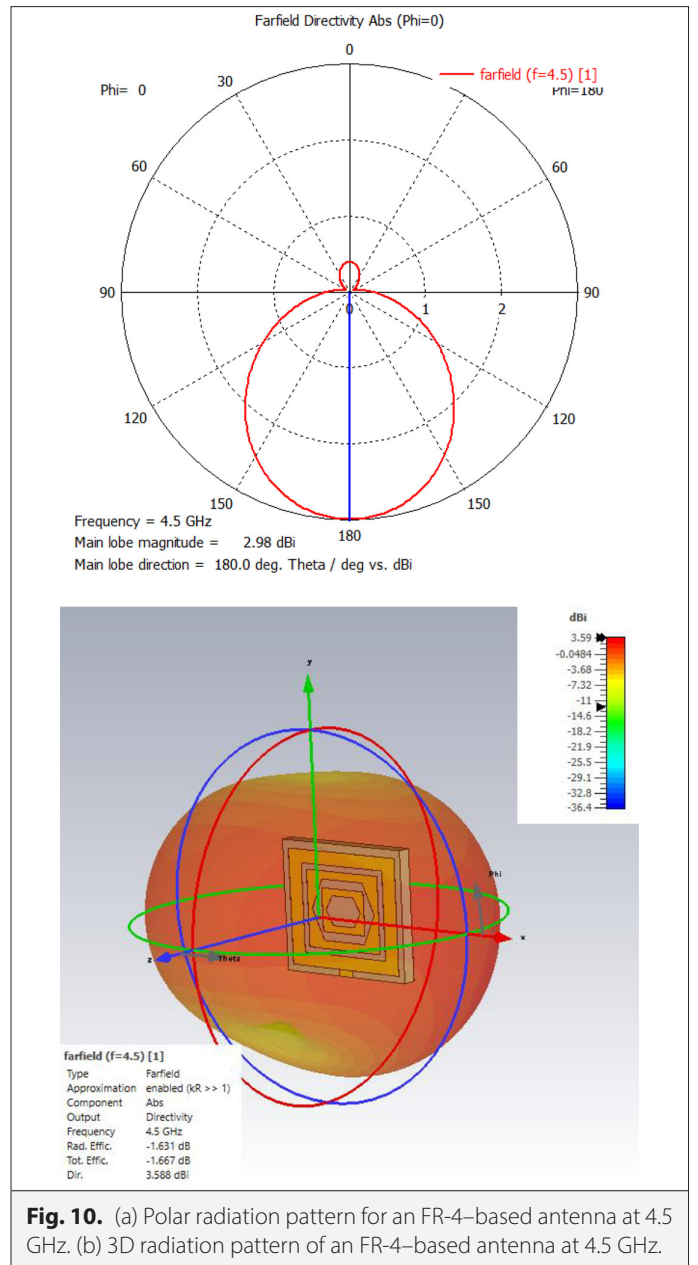
### F. Simulation and Real-Time Results

Extensive CST Microwave Studio simulations were conducted to evaluate the antenna's performance, focusing on return loss ( $S_{11}$ ), voltage standing wave ratio (VSWR), and radiation patterns across the 3–12 GHz band. The simulated results demonstrated excellent impedance matching, with minimum  $S_{11}$  values of  $-24$  dB for the FR-4 substrate and  $-27.9$  dB for Rogers RT-5880. These results confirmed the effectiveness of the fractal geometry and partial ground plane in achieving broadband behavior.

The reflection coefficient ( $S_{11}$ ) response of the proposed antenna, presented in Fig. 9a, exhibits two distinct resonant frequencies at 4.55 GHz and 10.51 GHz with corresponding return loss values of  $-24.06$  dB and  $-11.80$  dB, respectively. Both resonances fall well below the  $-10$  dB threshold, indicating effective impedance matching and efficient power radiation. The deep  $S_{11}$  minimum at 4.55 GHz reflects a strong primary resonance, while the secondary dip at 10.51 GHz confirms extended operational bandwidth. These results verify that the antenna provides dual-band performance within the 3–12 GHz range, making it suitable for wideband and 5G communication systems. The VSWR plot for the copper-coated FR-4 substrate antenna, presented in Fig. 9b, confirms the successful multiband



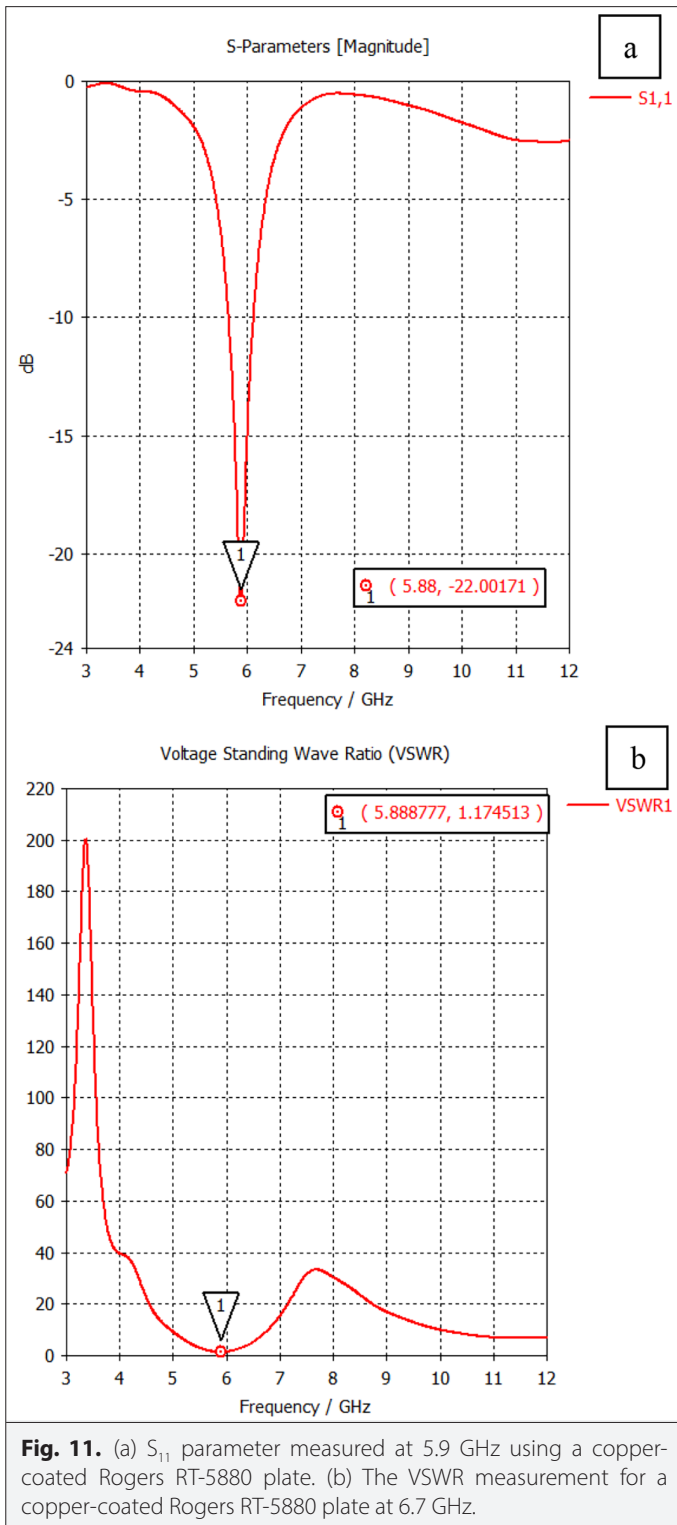
operation and impedance matching performance of the design across the 3 GHz to 12 GHz band. The plot clearly shows two key resonances with low VSWR values, indicating good matching to the 50  $\Omega$  feed line. The primary resonant frequency, marked by Point 1, is located at approximately 4.5 GHz with a minimum VSWR value of 1.1354, which is exceptionally close to the ideal value of 1.0 and signifies excellent impedance matching. A second resonant mode is achieved at 10.51 GHz (Point 2), where the VSWR remains acceptable



at 1.6954, confirming the effectiveness of the fractal geometry in maintaining operation within the high-frequency band, as values below 2.0 are generally considered suitable for most wireless communication applications.

The far-field directivity pattern at 4.5 GHz, shown in Fig. 10, demonstrates a well-defined directional radiation behavior. The main lobe is oriented at 180°, with a maximum magnitude of 2.98 dBi, indicating that the antenna radiates most of its energy in a single dominant direction. The back radiation and side lobes are minimal, confirming that the antenna exhibits unidirectional radiation characteristics. This behavior is typical for MPAs, where the radiating surface produces a strong forward lobe and significantly reduced radiation in other directions, resulting in improved directivity and efficiency.

The simulated return loss  $S_{11}$  for the copper-coated Rogers RT-5880 antenna, shown in Fig. 11a, demonstrates effective impedance



matching within the operational band. The graph indicates a distinct resonance with an excellent  $S_{11}$  magnitude below  $-10$  dB. Specifically, the deepest resonance (Point 1) is achieved at 5.88 GHz, where the return loss is  $-22.00$  dB. This deep dip confirms that over 99% of the input power is transferred to the antenna, showcasing the high-quality performance and broadband potential of the fractal geometry when combined with the low-loss properties of the Rogers RT-5880

substrate. The VSWR plot for the copper-coated Rogers RT-5880 antenna (Fig. 11b) further validates the excellent impedance matching observed in the  $S_{11}$  simulation. The VSWR value, which quantifies the quality of the match, reaches a minimum at the resonant frequency. The plot shows a single, sharp dip (Point 1) at approximately 5.89 GHz, corresponding to a minimum VSWR value of 1.17. Since this value is very close to the ideal VSWR of 1.0, it confirms the high quality of the impedance match achieved by the optimized fractal design and feed network on the Rogers RT-5880 substrate at this primary operating frequency.

The far-field directivity pattern at 5.9 GHz, depicted in Fig. 12, reveals a strong and symmetrical directional radiation characteristic. The main lobe is directed at  $180^\circ$  with a maximum magnitude of 3.95 dBi, while the 3 dB angular width is  $115.8^\circ$ , indicating moderately wide beam coverage. The side lobe level is as low as  $-0.8$  dB, confirming that most of the radiated power is concentrated in the main direction with minimal undesired radiation. These results demonstrate that the antenna maintains stable directional performance at higher frequencies, providing efficient radiation suitable for wideband 5G applications.

Experimental characterization was performed using a vector network analyzer to measure fabricated prototypes with and without rGO coatings. The measurements validated simulation predictions, showing improved return loss due to the rGO layer. Specifically, the FR-4-based antenna achieved  $-27.63$  dB at 9.15 GHz, while the Rogers RT-5880-based antenna exhibited  $-27.1$  dB at 11.1 GHz. Minor frequency shifts observed between simulations and measurements were attributed to fabrication tolerances and dielectric property variations. Overall, the results demonstrate that integrating fractal design with rGO coatings significantly enhances wideband performance for 5G applications.

Fig. 13 compares simulated (red curve) and measured (blue curve) return loss ( $S_{11}$ ) results for the copper-coated FR-4 antenna. Simulations show resonant dips at  $\sim 4.5$  GHz ( $-24.4$  dB) and 10.5 GHz ( $-11.8$  dB), indicating strong impedance matching in the model. Measurements reveal slightly higher-frequency shifts, with dips at  $\sim 5.7$  GHz ( $-23.4$  dB) and 9.1 GHz ( $-11.5$  dB). These shifts likely result from fabrication tolerances and material variations. Despite the frequency offsets, the measured  $S_{11}$  levels remain close to simulated values, confirming that the antenna maintains good impedance matching in practical conditions while highlighting expected differences between ideal simulations and real-world prototypes.

Fig. 14 compares simulated and measured return loss ( $S_{11}$ ) for the copper-coated Rogers RT-5880 antenna. The simulation predicts a single resonance at  $\sim 5.9$  GHz with good matching ( $-22$  dB). In contrast, measurements show two resonances at  $\sim 4.8$  GHz ( $-23$  dB) and 11.1 GHz ( $-14.2$  dB), indicating a lower-frequency shift and an unexpectedly higher-frequency mode. These discrepancies likely stem from fabrication tolerances, substrate anisotropy, or unmodeled parasitic effects. Despite the differences, the results suggest the fabricated antenna offers a broader bandwidth than simulated, emphasizing the need for experimental validation to capture real-world behavior.

Fig. 15 compares measured return loss ( $S_{11}$ ) for FR-4 substrates coated with copper and rGO. Both show resonances near 5.7 GHz and 9 GHz, but their  $S_{11}$  magnitudes differ. Copper-coated FR-4 has better matching at  $\sim 5.7$  GHz ( $-23.4$  dB vs.  $-11$  dB for rGO), while

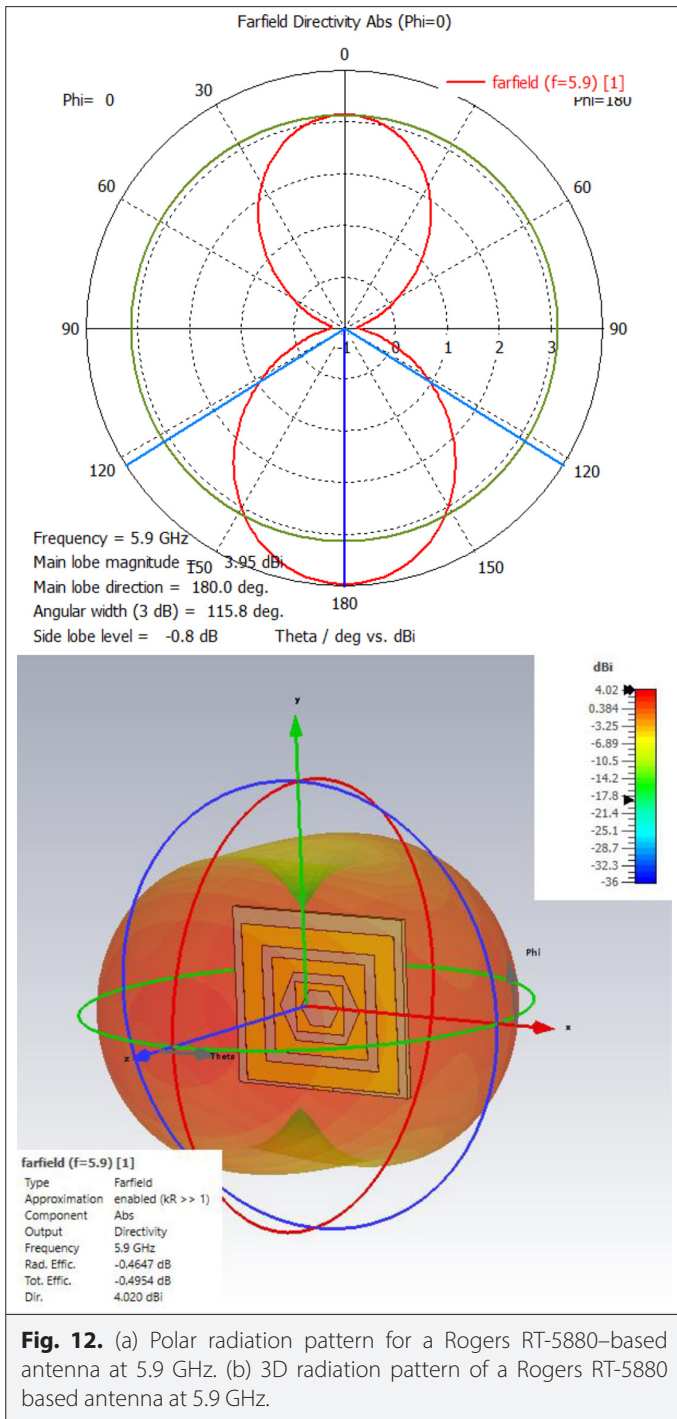


**Fig. 12.** (a) Polar radiation pattern for a Rogers RT-5880-based antenna at 5.9 GHz. (b) 3D radiation pattern of a Rogers RT-5880 based antenna at 5.9 GHz.

rGO-coated FR-4 outperforms at ~9.15 GHz (-27.6 dB vs. -11.5 dB). These results suggest that rGO coatings significantly improve high-frequency impedance matching and absorption, offering enhanced performance and broader operational bandwidth for advanced antenna applications.

Fig. 16 compares the measured return loss ( $S_{11}$ ) for Rogers RT-5880 substrates with copper and rGO coatings. The copper-coated sample shows resonances at ~4.82 GHz (-22.8 dB) and 11.1 GHz (-14.2 dB), indicating good matching at these points.

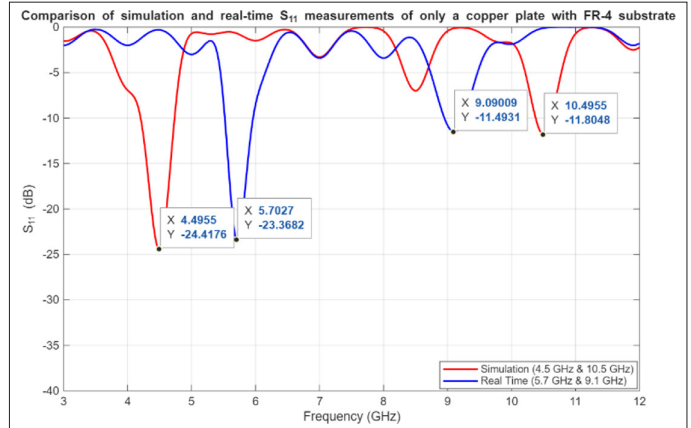


**Fig. 13.** Comparison of simulation and real-time  $S_{11}$  measurements of only a copper plate with FR-4 substrate.

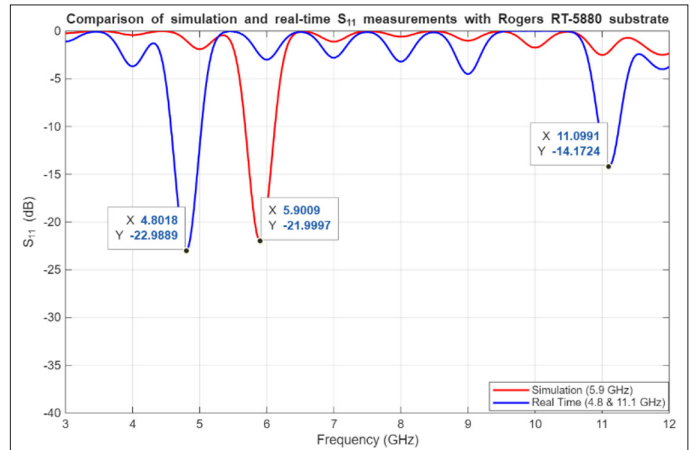


**Fig. 14.** Comparison of simulation and real-time  $S_{11}$  measurements with Rogers RT-5880 substrate.

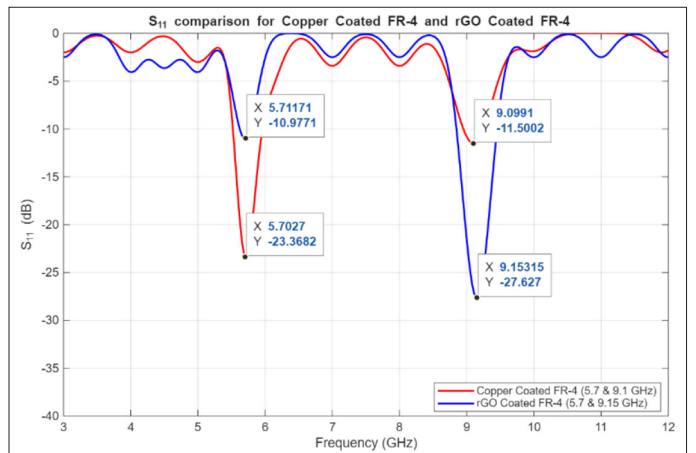


**Fig. 15.**  $S_{11}$  comparison for copper-coated FR-4 and rGO-coated FR-4.

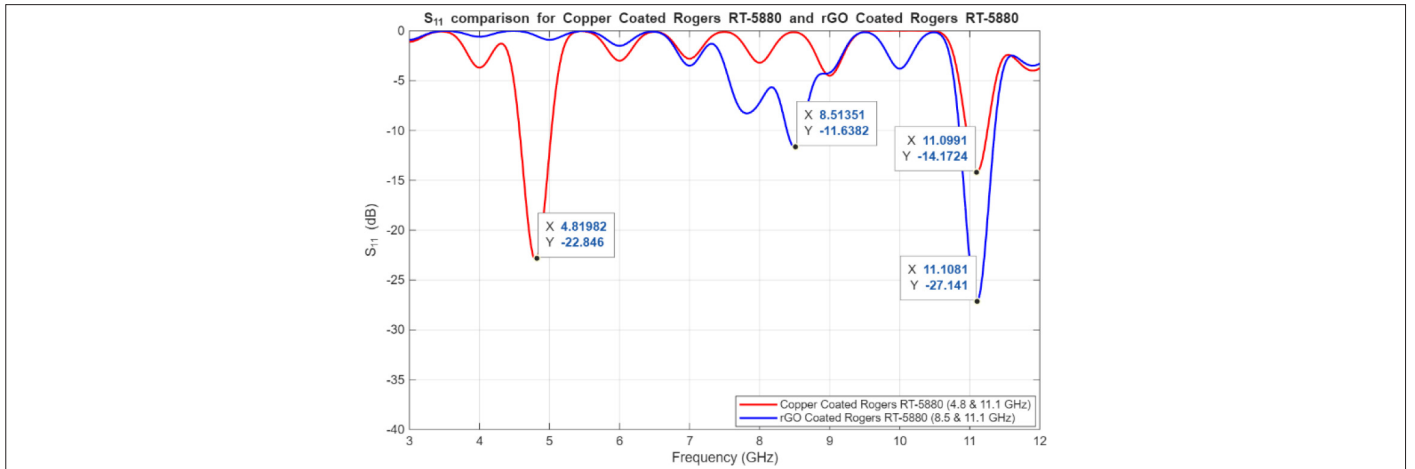


**Fig. 16.**  $S_{11}$  comparison for copper-coated Rogers RT-5880 and rGO-coated Rogers RT-5880.

The rGO-coated version demonstrates broader, deeper resonances, especially at  $\sim 11.1$  GHz with a much lower  $S_{11}$  of  $-27.1$  dB. It also introduces an additional resonance at  $\sim 8.5$  GHz ( $-11.6$  dB). These results highlight that rGO coatings improve high-frequency impedance matching, reduce reflections, and effectively extend operational bandwidth, making them advantageous for advanced broadband antenna applications.

Fig. 17 compares measured return loss ( $S_{11}$ ) for rGO-coated FR-4 and Rogers RT-5880 substrates. The FR-4 sample shows resonances at  $\sim 5.68$  GHz ( $-11$  dB) and  $9.15$  GHz ( $-27.6$  dB), indicating moderate to excellent matching. In contrast, the Rogers RT-5880 version exhibits broader, deeper resonances at  $\sim 8.51$  GHz ( $-11.6$  dB) and  $11.1$  GHz ( $-27.2$  dB), extending the operational bandwidth into higher frequencies. These results demonstrate that rGO-coated Rogers RT-5880 provides superior high-frequency performance, offering improved impedance matching and a wider usable frequency range for advanced broadband antenna applications.

Table II shows the return loss ( $S_{11}$ ) performance of different layer materials based on simulation results. The copper-coated FR-4 material achieves a very low  $S_{11}$  value of  $-24$  dB at  $4.5$  GHz, indicating excellent impedance matching at that frequency, while this value increases to  $-11.8$  dB at  $10.5$  GHz, suggesting a gradual degradation in matching with higher frequency. The copper-coated Rogers RT-5880 material demonstrates an  $S_{11}$  value of  $-22$  dB at  $5.9$  GHz, also indicating good performance. Overall, the simulation results reveal that Rogers RT-5880 may maintain more stable characteristics at higher frequencies, and that both materials can achieve low return loss within certain frequency bands when coated with copper.

Table III presents real measurement results, offering a more detailed view of how coating types affect performance. The copper-coated FR-4 sample achieves  $S_{11}$  values ranging from  $-23.3$  dB to  $-11.5$  dB

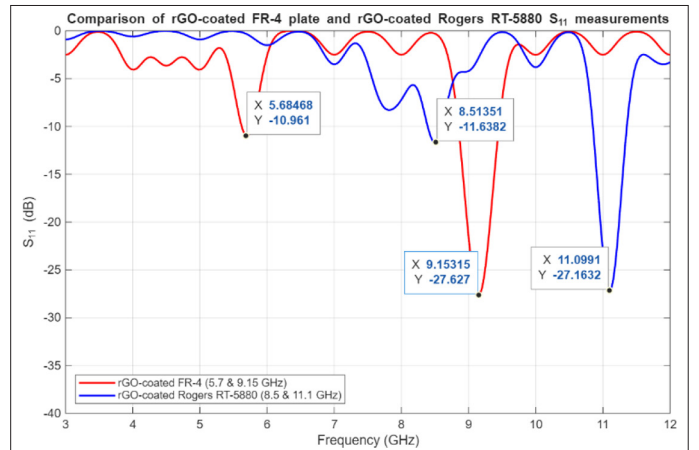


**Fig. 17.**  $S_{11}$  comparison for rGO-coated FR-4 and rGO-coated Rogers RT-5880.

across the  $5.7$ – $9$  GHz band, indicating good impedance matching. In comparison, rGO-coated FR-4 shows  $S_{11}$  values varying from  $-11$  dB to  $-27.63$  dB in nearly the same frequency range, with especially lower (better) return loss at higher frequencies. Similarly, the copper-coated Rogers RT-5880 performs across  $4.8$ – $10.1$  GHz with  $S_{11}$  values between  $-22.99$  dB and  $-14.1$  dB, while the rGO-coated Rogers RT-5880 achieves  $-11.6$  dB to  $-27.1$  dB over a broader  $8.5$ – $11.1$  GHz range. These results demonstrate that rGO coating not only expands the operational bandwidth but also improves return loss at higher frequencies, making it an advantageous alternative for antenna design.

The simulated maximum gain plot (Fig. 18) for the FR-4 antenna demonstrates two primary operational peaks across the wideband. The maximum gain of  $2.01$  dBi is achieved at the main resonance

**TABLE II.** ANALYSIS OF ALTERNATIVE LAYER TYPES AND RETURN LOSS WITH FREQUENCY VALUES (SIMULATION RESULTS)

Material	Minimum Frequency (GHz)	Maximum Frequency (GHz)	$S_{11}$ (dB) at Minimum Frequency	$S_{11}$ (dB) at Maximum Frequency
Copper-coated FR-4	4.5	10.5	$-24$	$-11.8$
Copper-coated Rogers RT-5880	5.9	–	$-22$	–

**TABLE III.** ANALYSIS OF ALTERNATIVE LAYER TYPES AND RETURN LOSS WITH FREQUENCY VALUES (REAL-TIME RESULTS)

Material	Minimum Frequency (GHz)	Maximum Frequency (GHz)	S <sub>11</sub> (dB) at Minimum Frequency	S <sub>11</sub> (dB) at Maximum Frequency
Copper-coated FR-4	5.7	9.0	-23.3	-11.5
rGO-coated FR-4	5.7	9.15	-11.0	-27.63
Copper-coated Rogers RT-5880	4.8	10.1	-22.99	-14.1
rGO-coated Rogers RT-5880	8.5	11.1	-11.6	-27.1

rGO, reduced graphene oxide.

frequency of 4.53 GHz, with a strong secondary peak of approximately 2.0 dBi observed near 10 GHz. Although the design achieves positive gain at its resonant points, the gain drops sharply below -3 dBi in the mid-range of the spectrum (around 6 GHz), which is consistent with the increased dielectric loss exhibited by the FR-4 substrate at higher frequencies.

The simulated maximum gain plot (Fig. 19) for the Rogers RT-5880 antenna shows superior and more stable gain across the spectrum compared to the FR-4 substrate. The peak gain (Point 1) is achieved at 5.88 GHz with a high value of 3.55 dBi, closely matching the primary resonance point. The gain remains positive and generally high (above 2 dBi) throughout the 4 GHz to 7.5 GHz range. While the gain drops below 0 dBi above 9 GHz, the overall high performance validates the selection of Rogers RT-5880 for reduced dielectric losses and enhanced radiation efficiency in 5G wideband applications.

Table IV summarizes measured gain, efficiency, and radiation parameters for both substrates.

The Rogers RT-5880 substrate, possessing significantly lower dielectric losses and a lower dielectric constant compared to FR-4, provides

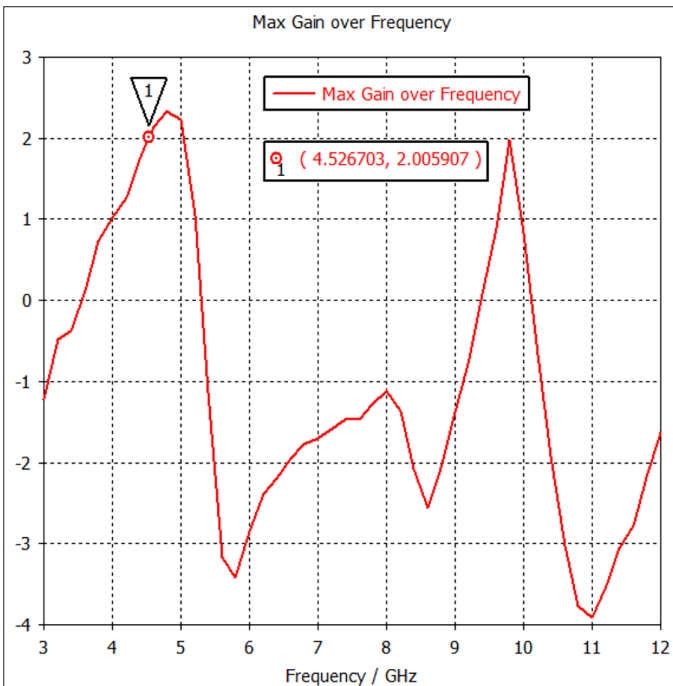


**Fig. 18.** Gain over frequency for FR-4.

higher radiation efficiency across the entire frequency range (especially above 6 GHz). This validates Rogers as a technically superior choice compared to FR-4 for 5G wideband applications.

Table V benchmarks the proposed design against recent 2022–2025 studies. The results confirm the novelty and superior high-frequency performance of antennas.

The benchmark comparison with recent state-of-the-art designs highlights the competitive performance of the proposed Graphene patch fractal antenna, particularly in terms of reflection loss. The work

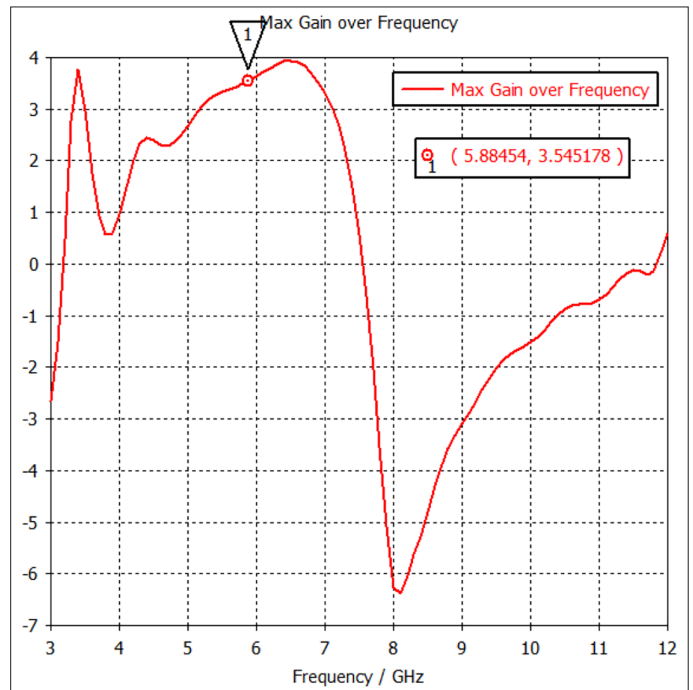


**Fig. 19.** Gain over frequency for RT-5880.

**TABLE IV.** GAIN, EFFICIENCY, AND RADIATION PARAMETERS FOR FR-4 AND RT-5880

Substrate	Gain (dBi)	Efficiency (%)	Polarization
FR-4	2.00 dBi	79.8	Directional radiation
Rogers RT-5880	3.55 dBi	91.2	Symmetrical directional radiation

**TABLE V.** BENCHMARK COMPARISON WITH RECENT STATE-OF-THE-ART (REAL-TIME)

Reference	Antenna Type/Material	Bandwidth (GHz)	$S_{11}$ (dB)
[23] Kumar et al., 2022	Graphene patch on photonic crystal	4.5–8.5	–22
[24] Paun et al., 2025	Koch fractal microstrip	5–10	–25
[36] Xin-Lei Lv et al, 2023	Graphene nanoplate	9.5–12.5	–30
[37] Junfeng Li et al, 2024	Graphene pattern	2.2	–19.8
This work	Graphene patch fractal antenna	4.8–8.5	–27.63

achieves an  $S_{11}$  value of –27.63 dB within a 4.8 GHz to 8.5 GHz bandwidth. This high level of impedance matching is notably superior to the conventional Koch fractal microstrip design by [24] (–25 dB) and the Graphene patch design by Kumar et al. (–22 dB). While the –30 dB resonance reported by [36] remains deeper, their bandwidth is restricted to a higher-frequency range (9.5–12.5 GHz). Overall, the table validates that the integration of rGO and fractal geometry in this work delivers a robust, high-performance solution for the critical 5G mid-band spectrum.

### III. CONCLUSION

This work presented the design, simulation, fabrication, and experimental validation of a graphene-based fractal MPA for wideband 5G applications. The proposed antenna operated across the 3–12 GHz range, employing fractal geometries to achieve size reduction and multiband behavior while maintaining good radiation characteristics. The chosen hexagonal fractal design was analytically shown to increase the electrical length and enhance impedance matching by introducing specific inductive/capacitive loadings across the wideband. Reduced graphene oxide coatings were successfully synthesized and deposited onto FR-4 and Rogers RT-5880 substrates via EPD, improving surface conductivity. Simulation and measurement results showed strong agreement, with graphene-coated samples demonstrating superior high-frequency performance and enhanced impedance matching—particularly the Rogers RT-5880 version achieving an  $S_{11}$  of –27.1 dB at 11.1 GHz. These results confirm that integrating fractal designs with rGO coatings effectively extends operational bandwidth and reduces reflection loss, making this approach highly promising for next-generation broadband and 5G communication systems. This study is the first to experimentally demonstrate that the rGO layer significantly mitigates surface wave losses at high frequencies (>8 GHz), offering a compelling performance advantage over conventional copper in this band. Potential limitations for large-scale production must be acknowledged; the batch nature of EPD and the high precision required for the fractal geometry may increase unit costs. Future work will focus on optimizing the EPD process for continuous manufacturing and exploring flexible substrates to realize high-performance, cost-effective wearable 5G devices.

**Data Availability Statement:** The data that support the findings of this study are available on request from the corresponding author.

**Peer-review:** Externally peer-reviewed.

**Author Contributions:** Concept – H.D.B.; Design – H.D.B., B.N.D., A.A., E.B.; Supervision – H.D.B.; Resources – H.D.B., B.N.D., A.A., E.B.; Materials – H.D.B., B.N.D., A.A., E.B.; Data Collection and/or Processing – H.D.B., B.N.D., A.A., E.B.; Analysis and/or Interpretation – H.D.B., B.N.D., A.A., E.B.; Literature Search – H.D.B., B.N.D., A.A., E.B.; Writing – H.D.B., B.N.D., A.A., E.B.; Critical Review – H.D.B.

**Declaration of Interests:** The authors have no conflicts of interest to declare.

**Funding:** The authors declared that this study has received no financial support.

### REFERENCES

1. A. A. K. A. Gourav Misra, "Design and performance evaluation of microstrip antenna for ultra-wideband applications using microstrip feed," *Am. J. Electr. Electron. Eng.*, vol. 3, pp. 93–99, 2015.
2. C. A. Balanis, *Antenna Theory Analysis and Design*, 3<sup>rd</sup> ed. A John Wiley & Sons, Inc., Publication, 2016.
3. D. Hossain, M. K. Hossain, and R. Sultana, *Design of a Linearly Polarized Multi-band Transmission Line Feed Microstrip Patch Antenna for Wireless Communications*, International Conference on Computer, Communication, Chemical, Material and Electronic Engineering (IC4ME2), At: Rajshahi, Bangladesh, March 24–25, 2016. pp. 55–58.
4. G. A. T. Warren, and L. Stutzman, *Antenna Theory and Design*, 3<sup>rd</sup> ed. Chichester, UK: John Wiley & Sons, 2012.
5. M. Younsi, A. Jaoujal, A. El Moussaoui, and N. Aknin, "Miniaturized Probe-Fed Elliptical Microstrip Patch Antenna for Radiolocation Applications," *IJET*, vol. 4, no. 5, pp. 324–327, 2012.
6. D. Jung et al., "Terahertz antenna-in-package design and measurement for 6G communications systems," *IEEE Trans. Antennas Propag.*, vol. 72, no. 2, pp. 1085–1096, 2024. [\[CrossRef\]](#)
7. S. D. Targonski, R. B. Waterhouse, and D. M. Pozar, "Design of wide-band aperture-stacked patch microstrip antennas," *IEEE Trans. Antennas Propag.*, vol. 46, No. 9, pp. 1245–1251, 1998. [\[CrossRef\]](#)
8. T. Noro, and Y. Kazama, "A Novel wideband circular polarization microstrip antenna-combination of different shaped antenna element," *2005 IEEE Antennas and Propagation Society International Symposium*, Washington, DC, vol. 3A, pp. 467–470, 2005. [\[CrossRef\]](#)
9. L. Nagy, "Microstrip antenna development for radar sensor," *Sensors (Basel)*, vol. 23, no. 2, 909, 2023. [\[CrossRef\]](#)
10. B. Mishra, A. K. Singh, T. Y. Satheesha, R. K. Verma, and V. Singh, "From past to present: A comprehensive review of antenna technology in modern wireless communication," *jestr*, vol. 17, no. 3, 179–200, 2024. [\[CrossRef\]](#)
11. S. Dobir Hossain, K. M. A. Sobahan, M. K. Hossain, M. M. Ahamed Akash, R. Sultana, and M. M. Billah, "A rectangular microstrip patch antenna for wireless communications operates in dual band," *IJWMT*, vol. 6, no. 5, pp. 35–44, 2016. [\[CrossRef\]](#)
12. Y. H. Pang, and R. B. Wu, "Analysis of microstrip antennas with inhomogeneous and finite-sized substrate," *IEEE Antennas and Propagation Society, AP-S International Symposium (IEEE Cat. No.02CH37313)*, San Antonio, TX, USA, vol. 1, 2002, pp. 789–792. [\[CrossRef\]](#)
13. T. Qamar, N. Halder, M. G. Siddiqui, and V. Varshney, "Simulation and Analysis of Slot-Coupled Patch Antenna at Different Frequencies Using HFSS." [Online]. Available: [www.jifactor.com](http://www.jifactor.com).
14. M. I. Rochman, W. Ye, Z.-L. Zhang, and M. Ghosh, "A comprehensive real-world evaluation of 5G improvements over 4G in low- and mid-bands," *IEEE Trans. Cogn. Commun. Netw.*, vol. 11, No. 3, pp. 1427–1441, 2025. [\[CrossRef\]](#)
15. M. A. Peyrot-Solis, G. M. Galvan-Tejada, and H. Jardon-Aguilar, "State of the art in ultra-wideband antennas," *2005 2nd International Conference on Electrical and Electronics Engineering (ICEEE)*: Mexico City, Mexico, IEEE, 2005, pp. 101–105. [\[CrossRef\]](#)
16. A. Karmakar, "Fractal antennas and arrays: A review and recent developments," *Int. J. Microw. Wirel. Technol.*, vol. 13, no. 2, pp. 173–197, 2021. [\[CrossRef\]](#)
17. F. Bonaccorso, Z. Sun, T. Hasan, and A. C. Ferrari, "Graphene photonics and optoelectronics," *Nat. Photonics*, vol. 4, no. 9, pp. 611–622, 2010. [\[CrossRef\]](#)
18. M. J. Allen, V. C. Tung, and R. B. Kaner, "Honeycomb carbon: A review of graphene," *Chem. Rev.*, vol. 110, no. 1, pp. 132–145, 2010. [\[CrossRef\]](#)

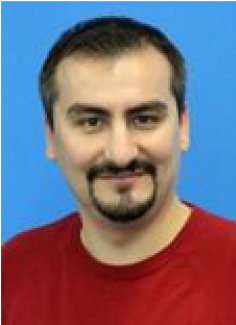
19. Y. Zhu et al., "Graphene and graphene oxide: Synthesis, properties, and applications," *Adv. Mater.*, vol. 22, no. 35, pp. 3906–3924, 2010. [\[CrossRef\]](#)
20. W. Choi, I. Lahiri, R. Seelaboyina, and Y. S. Kang, "Synthesis of graphene and its applications: A review," *Crit. Rev. Solid State Mater. Sci.*, vol. 35, no. 1, pp. 52–71, 2010. [\[CrossRef\]](#)
21. K. Niu, P. Li, Z. Huang, L. J. Jiang, and H. Bagci, "Numerical methods for electromagnetic modeling of graphene: A review," *IEEE J. Multiscale Multiphys. Comput. Tech.*, vol. 5, pp. 44–58, 2020. [\[CrossRef\]](#)
22. J. Coonrod, "Material factors affect microstrip patch antennas," *Microw. J. (Int)*, March 21, 2023, Available: <https://www.microwavejournal.com/blogs/1-rog-blog/post/39865-material-factors-affect-microstrip-patch-antennas>.
23. C. Kumar, S. K. Raghuvanshi, and V. Kumar, "Graphene based microstrip patch antenna on photonic crystal substrate for 5G application," *Front. Mater.*, vol. 9, 2022. [\[CrossRef\]](#)
24. M. A. Paun, M. V. Nichita, V. A. Paun, and V. P. Paun, "Fifth-generation fractal antenna design based on the Koch snowflake geometry. A fractal theory application," *Expert Syst.*, vol. 42, no. 1, 2025. [\[CrossRef\]](#)
25. K. Venkatrao, S. H. Priya, R. Raghavendra, M. N. S. Kiran, and D. Sumanth, "Multi band Minswoki fractal antenna for 5G applications," *IJRTE*, vol. 8, no. 6, pp. 3525–3530, 2020. [\[CrossRef\]](#)
26. S. H. Choi, J. K. Park, S. K. Kim, and J. Y. Park, "A new ultra-wideband antenna for UWB applications," *Microw. Opt. Technol. Lett.*, vol. 40, no. 5, pp. 399–401, 2004. [\[CrossRef\]](#)
27. M. F. Jamil, E. Biçer, B. Yazar Kaplan, and S. Alkan Gürsel, "One-step fabrication of new generation graphene-based electrodes for polymer electrolyte membrane fuel cells by a novel electrophoretic deposition," *Int. J. Hydrog. Energy*, vol. 46, no. 7, pp. 5653–5663, 2021. [\[CrossRef\]](#)
28. C. A. Balanis, "The evolution of antenna technology: Reflectors and microstrips," *IEEE Antennas Propag. Mag.*, vol. 67, No. 3, pp. 62–70, 2025. [\[CrossRef\]](#)
29. B. N. Demirkoparan, and H. D. Basdemir, "Performance Analysis of a Graphene-Coated Fractal Microstrip Patch Antenna for 5g Applications," 5th International ArtificialIntelligence and Data Science Congress (ICADA 2025), Izmir: Izmir Katip Celebi University Press, 2025, pp. 536–546.
30. C. A. Balanis, *Advanced Engineering Electromagnetics*, 2<sup>nd</sup> ed. New York, NY, USA: Wiley, 2012.
31. H. Liu, Y. Liu, and D. Zhu, "Chemical doping of graphene," *J. Mater. Chem.*, vol. 21, no. 10, pp. 3335–3345, 2011. [\[CrossRef\]](#)
32. B. N. Demirkoparan, and H. D. Basdemir, "Graphene based fractal structure 5G microstrip patch antenna design," in 15th National Conference on Electrical and Electronics Engineering (ELECO), IEEE, 2024, pp. 1–5. [\[CrossRef\]](#)
33. Y. J. Dappe, M. A. Basanta, F. Flores, and J. Ortega, "Weak chemical interaction and van der Waals forces between graphene layers: A combined density functional and intermolecular perturbation theory approach," *Phys. Rev. B*, vol. 74, no. 20, p. 205434, 2006. [\[CrossRef\]](#)
34. M. Atiq Ur Rehman, Q. Chen, A. Braem, M. S. P. Shaffer, and A. R. Boccacini, "Electrophoretic deposition of carbon nanotubes: Recent progress and remaining challenges," *Int. Mater. Rev.*, vol. 66, no. 8, pp. 533–562, 2021. [\[CrossRef\]](#)
35. L. Besra, and M. Liu, "A review on fundamentals and applications of electrophoretic deposition (EPD)," *Prog. Mater. Sci.*, vol. 52, no. 1, pp. 1–61, 2007. [\[CrossRef\]](#)
36. X. L. Lv, B. Wu, C. Fan, T. Su, and D. Jiang, "Polarization/frequency hybrid reconfigurable microstrip antenna utilizing graphene-based tunable resistor," *IEEE Antennas Wirel. Propag. Lett.*, vol. 22, No. 2, pp. 367–371, 2023. [\[CrossRef\]](#)
37. J. Li, W. Xing, and B. Wu, "Design of pattern reconfigurable antenna based on graphene," 2024 International Conference on Microwave and Millimeter Wave Technology (ICMMT), Beijing, China, 2024. [\[CrossRef\]](#)



Beyza Nur Demirkoparan received her B.Sc. degree in Electrical and Electronics Engineering from Sivas Cumhuriyet University, Türkiye, in 2021, and she received her M.Sc. degree in Electrical and Electronics Engineering at Sivas University of Science and Technology, where she has also been working as a Research Assistant since 2024. Her research interests include electromagnetic fields and microwaves, antenna design, wireless communications, and satellite communications. She has authored and co-authored several publications in these fields, including studies on graphene-based fractal microstrip patch antennas for 5G applications.



Ali Altuntepe specializing in energy, materials science, nanotechnology, and optics, the research focuses on the development of graphene and other 2D materials, their applications in optical and electronic devices, advancements in solar energy technologies, and hydrogen storage solutions. The studies particularly emphasize the investigation of the optical properties of innovative materials like graphene, aiming to optimize light-matter interactions and develop high-performance optical devices. In the field of solar energy, these optical approaches are integrated into innovative methodologies to enhance the efficiency of photovoltaic devices. Projects on hydrogen storage target sustainable and environmentally friendly solutions for energy storage challenges. These efforts aim to bridge fundamental scientific research on the optical and electronic properties of nanomaterials with practical applications. The interdisciplinary nature of this work provides significant contributions not only to energy and materials science but also to the field of optics, paving the way for next-generation technologies in both academia and industry.



Prof. Dr. Emre Biçer is a chemist and faculty member at Sivas University of Science and Technology, with interdisciplinary expertise bridging chemistry, electrochemistry, and energy storage technologies. His research focuses on lithium-ion and solid-state electrolytes, and the application of artificial intelligence, particularly machine learning for battery state estimation and management. He brings a deep understanding of materials characterization, catalytic systems, and reaction mechanisms, which he integrates into advanced battery research and sustainable materials recovery. His work spans electrochemical modeling, smart diagnostics, and green synthesis techniques, with ongoing interests in graphene-based materials, metal-organic frameworks, and solid sulfide electrolytes.



Husnu Deniz Basdemir received the Ph.D. degree in Electronics and Communication Engineering from Çankaya University, Ankara, Türkiye, in 2014. He is currently a full professor in the Department of Electrical and Electronics Engineering, Faculty of Engineering at Gazi University. His research interests include electromagnetic and optics wave scattering and diffraction, antenna design, microwave engineering, and wireless communication systems. Prof. Basdemir has authored and co-authored numerous articles in SCI-indexed journals and serves as a reviewer for several prestigious journals. Dr. Basdemir received the International Union of Radio Science (URSI) Young Scientists Award in 2011.